Journal of Solid State Chemistry 205 (2013) 57–63

Contents lists available at SciVerse ScienceDirect

Journal of Solid State Chemistry

journal homepage: www.elsevier.com/locate/jssc

Magnetocrystalline interactions and oxidation state determination of $Mn_{(2-x)}V_{(1+x)}O_4$ ($x=0$, 1/3 and 1) magnetorresistive spinel family

F. Pomiro [a], S. Ceppi [b], J.M. De Paoli [a,1], R.D. Sánchez [c,1], A. Mesquita [d], G. Tirao [b,*,1], E.V. Pannunzio Miner [a,**,1]

[a] INFIQC-CONICET, Departamento de Fisicoquímica, Facultad de Ciencias Químicas, Universidad Nacional de Córdoba, Ciudad Universitaria, 5000 Córdoba, Argentina
[b] IFEG-CONICET and Facultad de Matemática, Astronomía y Física, Universidad Nacional de Córdoba, Ciudad Universitaria, 5000 Córdoba, Argentina
[c] Centro Atómico Bariloche, Comisión Nacional de Energía Atómica e Instituto Balseiro, Universidad Nacional de Cuyo, 8400 San Carlos de Bariloche (RN), Argentina
[d] Instituto de Geociências e Ciências Exatas, Universidade Estadual Paulista, 13506-900 Rio Claro, São Pablo, Brazil

ARTICLE INFO

Article history:
Received 24 April 2013
Received in revised form
13 June 2013
Accepted 23 June 2013
Available online 10 July 2013

Keywords:
Cation distribution
High-resolution X-ray fluorescence
Electron paramagnetic resonance
X-ray absorption spectroscopy

ABSTRACT

Oxidation states of transition metal cations in spinels-type oxides are sometimes extremely difficult to determine by conventional spectroscopic methods. One of the most complex cases occurs when there are different cations, each one with several possible oxidation states, as in the case of the magnetoresistant $Mn_{(2-x)}V_{(1+x)}O_4$ ($x=0$, 1/3 and 1) spinel-type family. In this contribution we describe the determination of the oxidation state of manganese and vanadium in $Mn_{(2-x)}V_{(1+x)}O_4$ ($x=0$, 1/3,1) spinel-type compounds by analyzing XANES and high-resolution $K\beta$ X-ray fluorescence spectra. The ionic models found are $Mn_2^{2+}V^{4+}O_4$, $Mn_{5/3}^{2+}V_{4/3}^{3.5+}O_4$ and $Mn^{2+}V_2^{3+}O_4$. Combination of the present results with previous data provided a reliable cation distribution model. For these spinels, single magnetic electron paramagnetic resonance (EPR) lines are observed at 480 K showing the interaction among the different magnetic ions. The analysis of the EPR parameters show that g-values and relative intensities are highly influenced by the concentration and the high-spin state of Mn^{2+}. EPR broadening linewidth is explained in terms of the bottleneck effect, which is due to the presence of the fast relaxing V^{3+} ion instead of the weak Mn^{2+} (S state) coupled to the lattice. The EPR results, at high temperature, are well explained assuming the oxidation states of the magnetic ions obtained by the other spectroscopic techniques.

1. Introduction

In the design of oxides with potential technological applications, a detailed knowledge of the electronic configurations of the constituent elements plays an essential role. From the simple presence of magnetic correlations, to the more exotic phenomena related to them, all are controlled by the electronic structure of the material. The spinel case is very interesting in this regard and has been widely studied, as it shows a variety of effects due to different electronic correlations related to chemical composition (number of electrons) and crystal structure (where those electrons are located, and how they can interact with each other).

Materials belonging to the spinel family have an AB_2X_4 stoichiometry, where A and B are cations of either 2+ and 3+ charge or of 4+ and 2+ charge, and X represents O^{2-} or chalcogenides (like S^{2-} and Te^{2-}). The structure is based on the cubic close-packing of anions with the cations filling 1/8 of the tetrahedral (T_d) and 1/2 of the octahedral (O_h) sites. The general formula for the cationic distribution is $(A_{1-\gamma}B_\gamma)^{Td}\,[B_{2-\gamma}\,A_\gamma]^{Oh}\,O_4^{2-}$, were γ is the degree of inversion ($0\leq\gamma\leq1$) and T_d and O_h indicate tetrahedral and octahedral sites, respectively [1]. Besides, the octahedral sites are interconnected in a geometrically frustrated pyrochlore-type network.

Cation distribution between O_h and T_d sites is crucial, since it determines the magnetic and electrical properties of the spinels; thus, the knowledge of this distribution, as well as the oxidation state, is important to explain, control and predict the physical properties of this family of compounds [2,3].

Since the magnetoresistance effect (MR) was discovered in spinel-type oxides [4,5], these materials have been the subject of renewed studies in the field of material sciences. A few years ago we succeeded in synthesizing a family of spinel-type oxides, $Mn_{(2-x)}V_{(1+x)}O_4$ ($x=0$, 1/3 and 1) [6,7]. The composition with $x=1$, which can be easily obtained, has been thoroughly studied

* Corresponding author. Fax: +54 351 433 4054.
** Corresponding author. Fax: +54 351 4334188.
E-mail addresses: gtirao@famaf.unc.edu.ar (G. Tirao), eminer@fcq.unc.edu.ar, hamsterquatch@gmail.com (E.V. Pannunzio Miner).
[1] Members of the Research Career of CONICET.

0022-4596/$ - see front matter © 2013 Elsevier Inc. All rights reserved.
http://dx.doi.org/10.1016/j.jssc.2013.06.025

[8–20]. Its properties can be satisfactorily explained assuming that Mn is divalent and V is trivalent, based on the most stable oxidation states for these metals and the coincidence with experimental evidence reported in [8–19]. Our objective was to substitute V^{3+} for V^{4+}, while keeping Mn as Mn^{2+}. This would allow us to study the effect of two types of cations, one with electrons located only in t_{2g} orbitals (V^{3+} and V^{4+}), and another one with electrons in e_g and t_{2g} orbitals (Mn^{2+}). However, the presence of V^{4+} was only inferred, and had not been confirmed up to now.

A MR effect was reported in a study of structural, magnetic and electrical transport properties of $Mn_{(2-x)}V_{(1+x)}O_4$ ($x=0$, 1/3 and 1), which belong to the spinel-type family [6,7]. Electrical conduction in these samples occurs through small polarons [7]. This, coupled with the magnetostriction studied for the end-member of the series with $x=1$ [16], suggests that magnetoresistance could be the result of the interaction of these two effects. To elucidate this important question it is necessary to determine the oxidation states and distribution between T_d and O_h sites of Mn and V.

Albeit neutron diffraction techniques are probably the most widely used method to determine cation distribution between O_h and T_d sites, the oxidation state determination is not trivial. Even after considering some other indirect evidences and the redox potentials of V and Mn, the results did not allow an unambiguous assignment of site occupancies and oxidation states [6,7].

In general, electron paramagnetic resonance (EPR) is a good technique for determining the oxidation state of diluted magnetic ions. On the contrary, in the spinel system described in this contribution, the interpretation of the paramagnetic resonance is not trivial because the magnetic ions (vanadium and manganese) are concentrated and their orbitals are overlapped, which improve the exchange interaction and it dominates over the Zeeman interaction. However, a careful analysis of the experimental parameters obtained from the resonance lines, as the magnetic field resonance, linewidth and EPR intensity, can give information to infer the oxidation state of the magnetic ions, the magnetic interactions involved in the system and the relative importance to determine the magnetic order observed.

In this contribution we present a detailed study of electron paramagnetic resonance spectra complemented with high-resolution X-ray emission spectroscopy (XES) and X-ray absorption spectroscopy (XAS), measured in members of the spinel family $Mn_{(2-x)}V_{(1+x)}O_4$ ($x=0$, 1/3 and 1), using synthetic standards with known oxidation states of Mn and V for comparison. Our objective is to determine oxidation states and discuss their implications on electrical and magnetic properties.

2. Experimental

2.1. $Mn_{(2-x)}V_{(1+x)}O_4$ ($x=0$, 1/3 and 1) spinels

These samples have been synthesized by solid state reaction in sealed evacuated quartz ampoules [6]. Symmetry and unit cell dimensions have been determined using high-resolution synchrotron X-ray powder diffraction (HRS-XRPD) patterns measured at room temperature (RT). Crystal structure, cation site occupancies and magnetic structure have been refined using neutron powder diffraction (NPD) patterns obtained at RT. The details of these studies are discussed in Ref. [6]. The electrical transport and magnetic properties of $Mn_{(2-x)}V_{(1+x)}O_4$ ($x=0$, 1/3 and 1) samples were reported previously in Ref. [7].

In the present work, XES, XAS and EPR data were collected exactly on the same samples studied in previous works [6,7].

2.2. Synthesis of XES and XAS standards samples

The Mn standard samples selected for XES and XAS measurements were the following spinel-type double oxides: $Mn_{(1+z)}Cr_{(2-z)}O_4$ and $Zn_{(1-z)}Mn_{(2+z)}O_4$ ($z=0$, 0.25, 0.5, 0.75 and 1). $MnCr_2O_4$ is a normal spinel and Mn^{2+} occupies the *A* site [21]; when the Mn/Cr ratio exceeds ½, the surplus of Mn ions replace Cr ions in the *B* site as Mn^{3+} [22,23]. $ZnMn_2O_4$ is also a normal spinel and Mn^{3+} occupies the *B* site [24,25]; when the Mn/Zn ratio is more than 2, excess Mn ions replace Zn ions in the *A* site as Mn^{2+} [26].

These standard for Mn were prepared by the traditional ceramic method, mixing stoichiometric amounts of the corresponding reagents and following the sequence described in Ref. [27].

Vanadium was standardized against V_2O_3 (99.9%, Anhedra), VO_2 (99.9%, Strem Chemicals) and V_2O_5 (99.9%, Strem Chemicals), because V-bearing spinels are rather difficult to synthesize and the products require an independent confirmation of the oxidation state of V.

Each product was checked by XRPD. Patterns were taken at RT between 10° and 100° (2θ) with an angular step of 0.02° (2θ) and a counting time of 7 s per step, using Cu$K\alpha$ radiation in a PANalytical X'Pert Pro diffractometer. The identity and purity of all the standards were checked by the Rietveld method using the FULL-PROF software [28].

2.3. XES measurements

High-resolution $K\beta$ spectra were obtained with a non-conventional spectrometer, based on quasi-back diffraction geometry, installed at the D12A-XRD1 beamline of the National Synchrotron Light Laboratory—LNLS (Campinas, Brazil) [29]. Other measurements were made using the same spectrometer at the *Facultad de Matemática, Astronomía y Física (FAMAF), Universidad Nacional de Córdoba, Argentina* [30]. It is based on a spherically focusing Si crystal analyser operated at nearly back-diffraction geometry, in 1:1 Rowland geometry, in order to achieve high energy resolution. This non-conventional spectrometer was previously used to measure high-resolution $K\beta$ spectra of several Cr and Mn compounds [30–32].

For measurements of Mn spectra, the whole spectrometer (sample holder, analyser and detector), installed at FAMAF was operated with a cobalt-target X-ray conventional tube, working at 37.5 kV and 40 mA, as irradiation source. The high-resolution $K\beta$ emission spectra were recorded using the (4 4 0) reflection of the Si (1 1 0) spherical analyzer. The Bragg angle corresponding to the Mn $K\beta_{1,3}$ line is 84.2° for the Si(4 4 0) reflection. With a spot size of 2.4 mm^2, the measured counting rate at the $K\beta_{1,3}$ line was around 2200 counts s^{-1}, and the signal-to-background ratio was better than 100. The resolution of this spectrometer was determined to be 0.8 eV for the Mn $K\beta_{1,3}$ line [29].

For measurements of V spectra, due to the low count rate, samples were excited by a 5.57 keV monochromatic X-ray beam at the LNLS synchrotron beamline. The energy analysis was performed by scanning the focusing Si(3 3 1) crystal analyzer around the V-$K\beta_{1,3}$ emission line. The analyzer Bragg angle corresponding to the V $K\beta_{1,3}$ line is 66.5° and the energy resolution was 10.5 eV for the V $K\beta_{1,3}$ line [29]. With a spot size of 3 mm^2, the measured counting rate at the $K\beta_{1,3}$ line was around 450 counts s^{-1}, and the signal-to-back ground ratio was better than 60.

The energy scale was calibrated using the value of the $K\beta_{1,3}$ line for Mn^0 and V^0 given by Bearden [33] ($K\beta_{1,3}$=6490.45 eV for Mn and 5427.29 eV for V). Each spectrum was normalized to the incident beam intensity in order to take into account beam fluctuations. For calculations, spectra were first normalized to a constant value for the maximum of the $K\beta_{1,3}$ line and a linear background was subtracted.

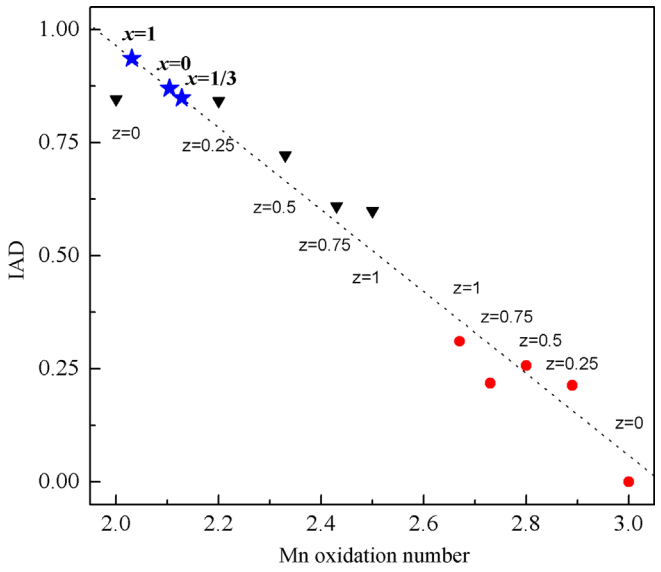

Fig. 1. IAD value as a function of oxidation number in $Zn_{(1-z)}Mn_{(2+z)}O_4$ (red circles) and $Mn_{(1+z)}Cr_{(2-z)}O_4$ (black triangle) for $z=0$, 0.25, 0.75, 1 spinels. The oxidation state of Mn in $Mn_{(2-x)}V_{(1+x)}O_4$ samples is obtained from the linear regression (dot line) of spinel series (see blue stars). The IAD errors are less than the dots dimension. (For interpretation of the references to color in this figure legend, the reader is referred to the web version of this article.)

2.4. XAS measurements

Mn *K* edge XAS spectra were acquired at the D04B-XAFS1 beamline of the LNLS. A Si(1 1 1) single channel-cut crystal monochromator with a slit aperture of 0.3 mm was used to obtain an energy resolution of about 1 eV [34]. The XAS spectra were collected in transmission mode. Energy calibration was performed by simultaneous absorption measurements on a Mn metal foil. Appropriate amounts of powered compounds were deposited on a cellulose membrane to reach an optimal sample thickness t_o for transmission experiments (edge jump close to 1). The t_o could be calculated as $\Delta\mu^{-1}$, where $\Delta\mu$ is the variation in the absorption coefficient before and after *K* edge. The calculation of the amount of sample was performed using the code MAX [35], which takes into account not only the metal contribution but also the contribution of the other elements present in the sample. Normalized XANES spectra were obtained by the Multiplatform Applications for XAFS code (MAX) [35].

2.5. EPR spectra measurements

EPR measurements were taken between 100 and 500 K with a microwave frequency of 9.44 GHz, corresponding to the X band, in a Bruker ESP-300 spectrometer. The powdered samples were mixed with KCl (1:3 ratio) in order to obtain a homogeneous microwave penetration and fill completely the cavity.

3. Results and discussion

3.1. Oxidation states of V and Mn determined using XES

Several spectral changes are related to the chemical environment surrounding the atoms of interest (Mn or V) [30,31]. In order to quantify the oxidation states, it is necessary to select those parameters that vary linearly, as evidenced from data collected on standards.

Table 1
Oxidation states of cations in the $Mn_{(2-x)}V_{(1+x)}O_4$ spinels determined using different spectral parameter from XES and XAS spectroscopy.

Sample	Manganese		Vanadium
	XES—IAD	XAS—Edge energy	XES—$IK\beta'$
Mn_2VO_4	(2.1 ± 0.2)	(2.1 ± 0.2)	(3.9 ± 0.3)
$Mn_{5/3}V_{4/3}O_4$	(2.1 ± 0.2)	(1.9 ± 0.2)	(3.2 ± 0.3)
MnV_2O_4	(2.0 ± 0.2)	(2.1 ± 0.2)	(2.8 ± 0.3)

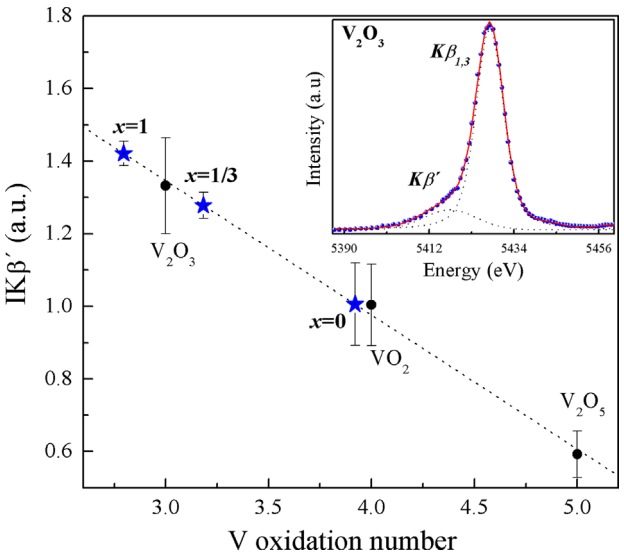

Fig. 2. $K\beta'$ intensity relative to the total intensity of the main $K\beta$ region ($K\beta'$ and $K\beta_{1,3}$ line) as a function of oxidation number in vanadium oxides (black circles). The oxidation state of V in $Mn_{(2-x)}V_{(1+x)}O_4$ samples (see blue stars) is obtained from linear regression (dot line). The inset shows the fitted data of V_2O_3 sample, as an example, by two Voigt functions in order to describer spectrum features. (For interpretation of the references to color in this figure legend, the reader is referred to the web version of this article.)

In the case of Mn compounds we used the integral of the absolute values of the difference spectra (hereafter IAD) value as reference parameters. The IAD [36] value for a spectrum with respect to a reference spectra $I_{ref}(E)$ is obtained with Eq. (1)

$$IAD = \int |I(E) - I_{ref}(E)| \partial E \quad (1)$$

The spectrum measured on $ZnMn_2O_4$ was considered as $I_{ref}(E)$. For IAD parameter, the oxidation states of the unknown samples were determined using a best-fit line, as shown in Fig. 1. The IAD data errors were calculated based on the IAD definition considering that statistical spectral errors were smaller than the spot size. The IAD parameter uses the whole spectrum information. The measured spectra only need simple pre-analysis steps: area normalization and $K\beta$1,3 line alignment. The oxidation states for the studied spinels are presented in Table 1. Observing the Eq. (1) it can be clearly seen that this parameter is proportional to the nominal spin N_s (see Ref. [36]). Taking into account that for Mn compounds in a high spin state, N_s is related to the oxidation state of manganese (O_{Mn}) by $N_s = 7 - O_{Mn}$, the IAD tendency must have a linear relationship with a negative slope, as shown in Fig. 1.

For V compounds it was not possible to use the same parameters as for Mn due to resolution limitations. Instead, we used the intensity of the $K\beta'$ line relative to the total area (hereafter $IK\beta'$). The $IK\beta'$ value was obtained by fitting the spectrum using two Voigt functions, in order to describe peaks features, as shown in the inset of Fig. 2. From the fitting parameters obtained, $IK\beta'$ was

calculated as the Voigt area corresponding to the $K\beta'$ line, divided by the sum of the Voigt areas corresponding to $K\beta'$ and $K\beta_{1,3}$ lines. The calculated $IK\beta'$ values for both standard and unknown samples are shown in Fig. 2, and display an inverse linear relationship with the oxidation state. This dependence can be explained using the simple model of Tsutsumi et al. [37], who pointed out that the $K\beta'$ intensity should be nearly proportional to the ratio between final state multiplicities, leading to $N_s/(N_s+1)$, where N_s is the nominal spin in the incomplete 3d shell. For V compounds $N_s=5-O_V$ and this explains the decreasing behaviour. The oxidation state of V in the unknown samples was determined using the calibration line as shown in Fig. 2.

3.2. Oxidation state of Mn determined using XAS

The edge energy was determined from the X-ray absorption spectrum in the usual way, i.e., half way up the normalized-edge step (i.e., where the absorption is equal to 0.5). A linear regression was made using standards with Mn of known oxidation states [38]. Two different linear tendencies were found corresponding to each group of standard samples (Cr-bearing spinels and Zn-bearing spinels). In order to determine the oxidation state of Mn in the $Mn_{(2-x)}V_{(1+x)}O_4$ spinels, we selected the linear fit obtained using Cr-bearing spinels (see Fig. 3) because this group displays values of the absorption edge energy closest to those of the studied samples, and the crystallographic occupation of Mn is similar. The obtained values of oxidation numbers for the $Mn_{(2-x)}V_{(1+x)}O_4$ ($x=0$, 1/3 and 1) spinels are in very good agreement with the corresponding values found using XES techniques (see Table 1).

It is noteworthy that the oxidation states obtained for Mn using equations derived from standards containing Mn+Zn deviate more strongly from the results given by XES. This shows that Cr is a better proxy for V in the spinel structure than Mn or Zn, and highlights the need of standards as close to the unknowns as possible to obtain the most accurate values when using XAS.

3.3. General discussion of X-ray spectroscopic results

The oxidation state of cations in the $Mn_{(2-x)}V_{(1+x)}O_4$ spinels as determined using X-ray spectroscopy appear in Table 1. Emission and absorption data give almost the same oxidation state for Mn (close to 2+). The oxidation state of V is then fixed by charge-balance constraints to 3+ in the case of MnV_2O_4 and to 4+ for Mn_2VO_4. For the sample of intermediate composition ($x=1/3$) vanadium has an average oxidation state of 3.5+, due to the presence of equal amounts of V^{4+} and V^{3+}. All of these values are within the error of the values determined by XES. It should be stressed that no oxygen vacancies were detected in these spinels [6], so that a total negative charge of 8 can be safely assumed. Recently, the oxidation state of vanadium and manganese in $x=1$ spinel was determined using electron energy-loss spectroscopy [39]. The results presented in Ref. [39] are in complete agreement with our determination.

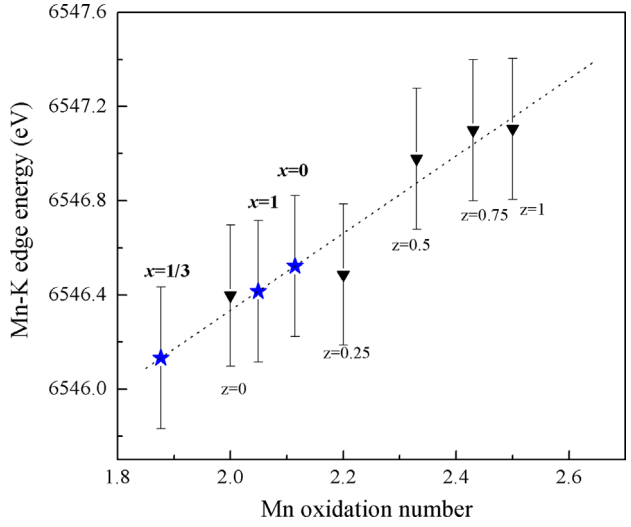

Fig. 3. Edge step position at the energy half way up of the normalized-edge step in the usual way for $Mn_{(1+z)}Cr_{(2-z)}O_4$ (black triangle) with $z=0$, 0.25, 0.5, 0.75, 1 spinels. A linear regression was made with known oxidation state. Oxidation state of Mn in $Mn_{(2-x)}V_{(1+x)}O_4$ samples is indicated by the blue stars. (For interpretation of the references to color in this figure legend, the reader is referred to the web version of this article.)

These $Mn_{(2-x)}V_{(1+x)}O_4$ spinels samples have been previously studied by NPD [6]. Therefore, the manganese and vanadium occupancies for each crystallographic site are well known. Considering these statements, the following ion distribution models can be proposed:

$x=0$, Mn_2VO_4: $[Mn^{2+}_{0.89}V^{4+}_{0.11}]^{Td}[Mn^{2+}_{1.11}V^{4+}_{0.89}]^{Oh}O_4$
$x=1/3$, $Mn_{5/3}V_{4/3}O_4$: $[Mn^{2+}]^{Td}[Mn^{2+}_{0.67}V^{4+}_{0.67}\ V^{3+}_{0.67}]^{Oh}O_4$
$x=1$, MnV_2O_4: $[Mn^{2+}_{0.75}V^{3+}_{0.25}]^{Td}[Mn^{2+}_{0.25}V^{3+}_{1.75}]^{Oh}O_4$

where T_d and O_h super-indices indicate tetrahedral and octahedral sites, respectively.

3.4. Electron paramagnetic resonance results

The X-band EPR spectra of $Mn_{(2-x)}V_{(1+x)}O_4$ ($x=0$, 1/3 and 1) compounds are shown in Fig. 4. The spectra were taken at approximately 480 K, normalized by the mass of sample and by receiver gain; only one line is observable in all of the samples, as expected for concentrated magnetic systems [40–42] The spectrum of the sample with $x=0$ is well fitted with a Lorentzian resonance shape, giving practically the same g-value and the resonance line-width (magnetic field difference between two peaks, ΔH_{pp}) parameters than those obtained from the experimental resonance

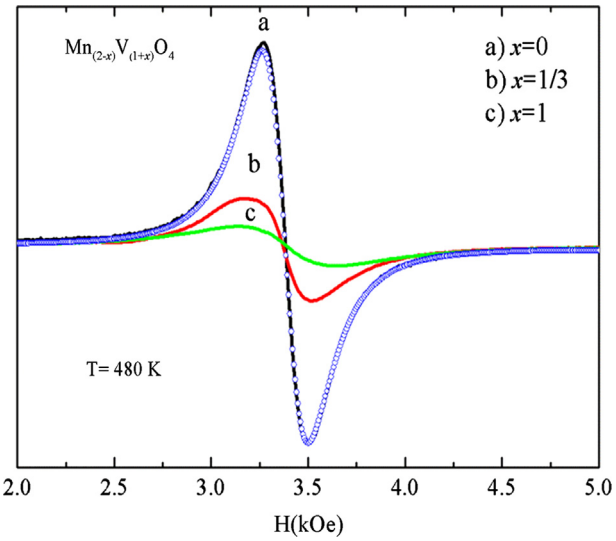

Fig. 4. X-band EPR spectra of $Mn_{(2-x)}V_{(1+x)}O_4$ ($x=0$, 1/3 and 1) recorded at 480 K. The solid lines are the experimental spectra. Note that the height difference (y) between consecutive peaks in the resonance spectra decreases with increasing x, and also that the magnetic field distance (ΔH_{pp}) between peaks is broadening. The a (black line in the on-line version) corresponds to $x=0$, b (red line on-line) to $x=1/3$ and c (green line on-line) to $x=1$, respectively. Open circles (blue on-line) represent the fit of the spectrum with $x=0$ using a single a Lorentzian curve shape. (For interpretation of the references to color in this figure legend, the reader is referred to the web version of this article.)

spectra. For other compositions, where the relative Mn^{2+} amount decreases and consequently the proportion of the other magnetic ions increases, it becomes more difficult to fit the spectra with a single Lorentzian curve.

With the increase of x, two effects can be clearly appreciated in Fig. 4: (i) the decrease of the height difference (y) between consecutive peaks, and (ii) the increase of ΔH_{pp}. For all of the samples, we observe a single line with a magnetic field resonance close to $H_r \approx 3380$ Oe. This experimental value corresponds approximately to a g-value ($g = h\nu/\mu_B H_r$) of 1.996.

The g-values (g_i) reported in the bibliography [43,44] are 1.965, 1.935 and 2.001 for the magnetic ions present in the samples, where $i = V^{4+}$, V^{3+} and Mn^{2+}, their respective spin numbers being $S_i = ½$, 1 and 5/2. In magnetic materials with two or more different magnetic species, such as these spinels, the exchange dominates over the Zeeman interaction and consequently only one line should be observed with an average g-value weighted by the individual factors of each species present. It is given by the Huber's equation [45]:

$$g = \frac{\sum_i g_i W_i}{\sum_i W_i} \quad (2)$$

where $W_i = M_i S_i(S_i+1)$ and M_i is the relative concentration of a given ion. Note that the high spin number of the Mn^{2+}, and consequently of its weight (W_i), are very important to determine the g-value average, which should be have a slightly shift from the free Mn^{2+} g-value. Experimental and calculated g-values using Eq. (2) are shown in Fig. 5a. The calculated values fall within the error bar of the experimental data. Similar magnetic coupling among magnetic species has been reported recently by Winkler et al. in the $MnCr_2O_4$ spinel [46].

The EPR intensity, normally called EPR susceptibility, can be estimated by $I_x = y\,(\Delta H_{pp})^2$, and similar values have been obtained with the double integral of the spectra. We normalized I_x with the intensity corresponding to the $x=1$ value, symbolized as $I_x/I_{x=1}$. The relative EPR intensity decreases with the diminution of manganese concentration in the samples (see values in Table 2 and Fig. 5b—right axis). The tendency of these values is in accordance with the stoichiometric amount of Mn^{2+} ion in each chemical formula: 2, 1.67 and 1 for $x=0$, 1/3 and 1, respectively. This also confirms that the principal contribution to the Mn–V resonance line comes from the Mn^{2+} ion ($S=5/2$).

The ΔH_{pp} values increase with the x values and it is shown in Fig. 5b (left axis). In concentrated magnetic systems, the EPR linewidth is related to the effective magnetic field, such that it increases with increased anisotropic contributions (dipole–dipole, inhomogeneities, exchange of magnetic impurities, H_A) and it is inversely proportional to the isotropic contributions (such as exchange interactions between neighbour magnetic ions, H_E); the effective magnetic field can be expressed as $\Delta H_{pp} \sim H_A^2/H_E$ [47].

In general, two different exchange interactions (J_{AB} and J_{BB}) are important to define the magnetic order in the AB_2O_4 spinels. The third exchange interaction, J_{AA}, is almost negligible compared with the magnitude of the other two, essentially because of the large A–A distance. J_{AB} is the exchange interaction between neighbour magnetic cations that occupy the tetrahedral (A, here labelled T_d) and the octahedral (B, here labelled O_h) sites, while J_{BB} is the corresponding exchange interaction between the transition metal ions located at the octahedral (O_h–O_h) sites. In cubic spinels, the A–O–B angle is approximately 126° and the B–O–B angle is 90°. Based upon the Goodenough–Kanamori rules, for the particular case where $3d^5$ ions occupy the A sites and the B sites are populated by $3d^n$ (with $n \leq 3$) ions, it can be expected that $J_{BB} > J_{AB}$, and the spin configuration will be non-collinear [48].

Structural refinements of these compounds using neutron diffraction show that the tetrahedral (A) site is virtually fully occupied by Mn^{2+} ($3d^5$) for all the studied compositions and $3d^n$ (with $n \leq 3$) ions are in the B site [6]. Also, in our previous study [7] we show that the magnetic order temperature (T_N) increases with x. As J_{BB} is the principal exchange interaction and $T_N \sim J_{BB}$, it should increase with x, with a concomitant linewidth narrowing [47]. However, our EPR results show the contrary effect: the broadening of the EPR linewidth with x, which strongly suggests another relaxation mechanism as the responsible for producing the ΔH_{pp} broadening.

One possible mechanism is the bottleneck effect [49], which occurs for example when a localized magnetic m-ion is weakly coupled to the lattice (L), as a Mn^{2+} or S-state ion, and a second n-ion is introduced in the host (sometimes as impurity) and it is strongly coupled to the lattice, providing an additional relaxation path. Therefore, the m-ion presents a slow relaxation rate to the lattice (δ_{mL}), but the n-ion is fast relaxing (δ_{nL}) to the lattice and it defines the linewidth broadening of the system ($\delta_{mL} \approx \delta_{nL}$). The extra parameters, $\delta_{mn} \approx \delta_{nm}$, are the spin–spin relaxation rate, resulting from the exchange interaction between the magnetic subsystems and $\delta_{nm} < \delta_{nL}$.

Now, taking as reference Mn_2VO_4 ($x=0$) with the S-state Mn^{2+} ions, which are partially (or totally, in the case of V^{4+}) replaced by

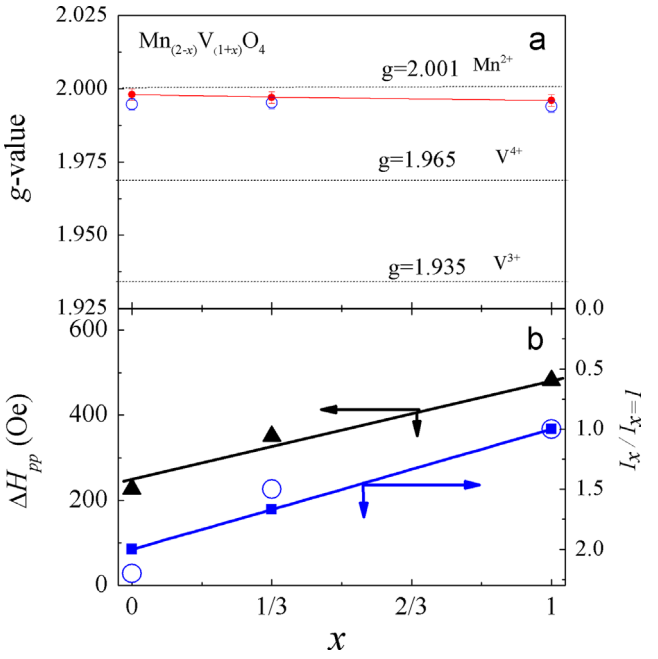

Fig. 5. Dependence of different parameters obtained from EPR spectra with x in $Mn_{(2-x)}V_{(1+x)}O_4$ samples. (a) g-value obtained from the resonance field of the spectra. Symbols with error bar (red on-line) correspond to experimental values and open circles (blue on-line) were calculated with Eq. (2) (see text). Dashed lines indicate the g-value expected for the corresponding manganese and vanadium ions. (b) On the left axis the EPR linewidth is represented (triangles). On the right axis, the relative EPR intensity (I_x), with respect to $x=1$, obtained comparing the intensity of the resonance lines and the expected value assuming that resonance is produced exclusively by Mn^{2+} ions (squares). (For interpretation of the references to color in this figure legend, the reader is referred to the web version of this article.)

Table 2
EPR parameters obtained from the spectra taken at $T=480$ K.

x	Hr (Oe)	y (arb. units)	ΔH_{pp} (Oe)	I_x (10^7)	$I_x/I_{x=1}$
0	3386(7)	1087(1)	226(14)	5.5(3)	2.2(2)
1/3	3371(7)	279(1)	351(14)	3.5(1)	1.5(2)
1	3386(7)	108(1)	485(14)	2.5(1)	1.0

V^{3+} ($S=1$) when x is increased. The experimental ΔH_{pp} broadening is due to this fast-relaxing magnetic ion (V^{3+} or V^{4+}), whose exchange rate determines the linewidth of the resonance. This argument is also supported by the observation of bottleneck effect in the $Zn[Cr_{2-x}V_x]Se_4$ spinel [50].

3.5. Comparison with previous magnetic, transport and structural data

The magnetic properties of these three oxides were studied by Pannunzio Miner et al. [6,7]. Data on oxidation states of Mn and V were not available by the time of that contribution, so two possible models of ionic distribution were examined using crystal-chemical arguments and compared against observed values for magnetic parameters.

The model favoured by those authors has been confirmed by the data presented here for two compositions (those with $x=1/3$ and 1), whereas the spinel with $x=0$ shows a better agreement with a different ionic distribution (proposed as $Mn^{2+}Mn^{3+}V^{3+}O_4$ [7]). For this compound, the observed C value calculated using a ferrimagnetic model of magnetization data is 8.56(3) emu/(K mol) [7]. This C value is lower than that obtained from theoretical calculations (10.4 emu/(K mol)) assuming a $Mn_2^{2+}V^{4+}O_4$ composition. In other words, the experimental μ_{eff} (obtained from the C value) is 8.27 μ_B mol^{-1}, i.e., lower than 9.12 μ_B mol^{-1} corresponding to the theoretical value for $Mn_2^{2+}V^{4+}O_4$. Since this latter ionic distribution model has been confirmed using spectroscopic methods, we can infer that some of the electrons are delocalized, with no contribution to the effective magnetic moment, as shown by the fact that is μ_{eff} theoretical higher than μ_{eff} observed. This is also supported by the study of electric transport carriers, which were shown to be different from that of the other two oxides. Seebeck experiments demonstrated, for the sample with $x=0$, that charge carriers are electrons, whereas for the other samples the charge carriers are holes [7].

From a structural point of view, the fact that all of Mn is present as Mn^{2+} (a d^5 spherical ion) suggests that the small tetragonal distortion shown by all of the samples at low temperature [6] is a consequence of the weak Jahn–Teller effect due to the presence of V^{3+} and V^{4+} ions.

4. Conclusions

The model regarding the oxidation states of V and Mn and the site occupancies in $Mn_{(2-x)}V_{(1+x)}O_4$ spinels proposed by Pannunzio Miner et al. [6,7] was refined using a combination of data taken from XAS, XES and EPR measurements. The combination of these techniques with powder neutron diffraction data is a powerful tool to determine univocally oxidation states in mixed oxides with variable oxidation states transition metal cations and thus, explain or predict magnetic and transport properties in these important family of compounds where important properties of technical applications can be found.

In this contribution we have confirmed the presence of V^{4+} in the $x=1/3$ and $x=0$ compositions and, consequently, the success of the synthesis design. Regarding the three empirical model previously reported, we have corroborated experimentally two of them [for $Mn_{5/3}V_{4/3}O_4$ ($x=1/3$) and MnV_2O_4 ($x=1$)], whereas a different model is more appropriate for Mn_2VO_4 ($x=0$).

In this spinel system, where the magnetic ions are concentrated and coupled, the EPR results at high temperatures show single paramagnetic resonances where their g-values are well described with an average of the free ion g-values weighted by the individual spin and relative ion concentrations. The EPR intensity parameter values show a high contribution of the Mn^{2+} ions present in the system. The EPR linewidth, which broadens with the increase of the amount of V^{3+} ions, shows how this ion introduces an additional fast relaxing way (bottleneck effect) to the weakly Mn^{2+} S-state coupled to the lattice.

Acknowledgments

The research was supported by LNLS-Brazilian Synchrotron Light Laboratory (projects D12A XRD1-9843, and D04B-XAFS1-10693). Financial supports from the *Consejo Nacional de Investigaciones Científicas y Técnicas* (CONICET), Agencia Nacional de promoción científica y tecnológica (ANPCyT) and from the *Secretaría de Ciencia y Tecnología de la Universidad Nacional de Córdoba* (UNC) are gratefully acknowledged. The authors thank R. E. Carbonio and F. Colombo and anonymous reviewers for helpful comments.

References

[1] Hk. Müller-Buschbaum, J. Alloys Compd. 349 (2003) 49.
[2] S.M. Yunus, H. Yamauchi, A.K.M. Zakaria, N. Igawa, A. Hoshikawa, Y. Haga, Y. Ishii, J. Alloys Compd 455 (2008) 98.
[3] B.E. Martin, A. Petric, J. Phys. Chem. Solids 68 (2007) 2262.
[4] A.P. Ramirez, R.J. Cava, J. Krajewski, Nature 386 (1997) 156.
[5] J. Philipp, T.R.N. Kutty, Mater. Lett. 39 (1999) 311.
[6] E.V. Pannunzio-Miner, J.M. De Paoli, R.D. Sánchez, R.E. Carbonio, Mat. Res. Bull. 44 (2009) 1586.
[7] E.V. Pannunzio-Miner, J.M. De Paoli, R.D. Sánchez, R.E. Carbonio, J. Appl. Phys. 105 (2009) 113906.
[8] B. Reuter, E. Riedel, P. Hug, D. Arndt, U. Geisler, J. Behnke, Z. Anorg, Allg. Chem 369 (1969) 306.
[9] J.C. Bernier, P. Poix, Ann. Chim. Paris (1967) 81.
[10] K. Adachi, T. Suzuki, K. Kato, K. Osaka, M. Takata, T. Katsufuji, Phys. Rev. Lett. 95 (2005) 197202.
[11] R. Plumier, M. Sougi, Physica B 155 (1989) 315.
[12] R. Plumier, M. Sougi, Solid State Commun. 64 (1987) 53.
[13] V.O. Garlea, R. Jin, D. Mandrus, B. Roessli, Q. Huang, M. Miller, A.J. Schultz, S.E. Nagler, Phys. Rev. Lett. 100 (2008) 66404.
[14] V. Hardy, Y. Be´ard, C. Martin, Phys. Rev. B: Condens. Matter 78 (2008) 24406.
[15] S.-H. Baek, K.-Y. Choi, A.P. Reyes, P.L. Kuhns, N.J. Curro, V. Ramanchandran, N.S. Dalal, H.D. Zhou, C.R. Wiebe, J. Phys. Condens. Matter 20 (2008) 135218.
[16] T. Kstsufuji, K. Adachi, T. Suzuki, M. Katsumura, Physica B 383 (2006) 13.
[17] T. Suzuki, M. Katsumura, K. Taiguchi, T. Arima, T. Katsufuji, Phys. Rev. Lett. 98 (2007) 127203.
[18] K. Miyoshi, M. Ihara, K. Fujiwara, J. Takeuchi, Physica B 281–282 (2000) 30.
[19] Y. Hu, Y.-H. Liu, Mater. Chem. Phys. 90 (2005) 255.
[20] T. Sonehara, K. Kato, K. Osaka, M. Takata, T. Katsufuji, Phys. Rev. B: Condens. Matter 74 (2006) 104424.
[21] J.M. Hastings, L.M. Corliss, Phys. Rev 126 (1962) 556–565;
J.M. Hastings, L.M. Corliss, J. Appl. Phys 33 (1962) 1138.
[22] S. Lucchesi, U. Russo, A. della Giusta, Eur. J. Mineral 9 (1997) 31.
[23] J.-L. Gautier, J. Ortiz, G. Zelada, G. Poillerat, J. Chim. Phys. PCB 86 (9) (1989) 1889.
[24] M. Nogues, P. Poix, Ann. Chim. (Paris) (1972) 301.
[25] M. Nogues, P. Poix, J. Phys. Chem. Solids 25 (1962) 711.
[26] F. Bosi, S. Lucchesi, A. della Giusta, Am. Mineral 87 (2002) 1121.
[27] H. Eba, K. Sakurai, J. Solid State Chem. 178 (2005) 370.
[28] J. Rodriguez-Carbajal, Physica B 192 (1993) 55.
[29] G. Tirao, G. Stutz, C. Cusatis, J. Synchrotron Radiat 11 (2004) 335.
[30] G. Tirao, S. Ceppi, A.L. Cappelletti, E.V. Pannunzio Miner, J. Phys. Chem. Solids 71 (2010) 199.
[31] S. Limandri, S. Ceppi, G. Tirao, G. Stutz, C.G. Sánchez, J.A. Riveros, Chem. Phys. 367 (2010) 93.
[32] M. Torres Deluigi, G. Tirao, G. Stutz, C. Cusatis, J.A. Riveros, Chem. Phys. 325 (2006) 477.
[33] J.A. Bearden, Rev. Mod. Phys. 39 (1967) 78.
[34] A. Ramos, Y. Tolentino, H., Alves, M.C.M., Energy Resolution at LNLS -XAS beamline Internal Report MeT-02/99, 1999.
[35] M. Alain, M. Jacques, M.-B. Diane, P.K. Michalowicz, J. Phys. Conf. Ser. 190 (2009) 012034.
[36] G. Vankó, T. Neisius, G. Molnár, F. Renz, S. Kárpáti, A. Shukla, F.M.F. de Groot, J. Phys. Chem. B 110 (2006) 11647.
[37] K. Tsutsumi, H. Nakamori, K. Ichikawa, Phys. Rev. B: Condens. Matter 13 (1976) 929.
[38] P. Chaurand, J. Rose, V. Briois, M. Salome, O. Proux, V. Nassif, L. Olivi, J. Susini, J.L. Hazemann, J.Y. Bottero, J. Phys. Chem. B 111 (2007) 5101.
[39] H. Tan, J. Verbeeck, A. Abakumov, G. Van Tendeloo, Ultramicroscopy 116 (2012) 24.
[40] S. Mandal, A. Ghosh, Phys. Rev. B: Condens. Matter 48 (1993) 9388.

[41] S. Gupta, N. Khanijo, A. Mansingh, J. Non-Cryst. Solids 181 (1995) 58.
[42] E. Dormann, D Hone, V. Jaccarino, Phys. Rev. B: Condens. Matter 14 (1976) 2715.
[43] G.E Pake, Paramagnetic Resonance: An Introductory monograph, W. A. Benjamin Inc., New York, 1962.
[44] K.D. Bowers, J. Owen, Rep. Prog. Phys 18 (1955) 304.
[45] D.L. Huber., Phys. Rev. B: Condens. Matter 12 (1975) 31.
[46] E. Winkler, S. Blanco Canosa, F. Rivadulla, M.A. López-Quintela, J. Rivas, A. Caneiro, M.T. Causa, M. Tovar, Phys. Rev. B: Condens. Matter 80 (2009) 104418.
[47] P.W. Anderson, P.R. Weiss, Rev. Mod. Phys. 25 (1953) 269.
[48] John B. Goodenough, in Magnetism and the Chemical Bond, Interscience (Wiley), New York, 1963.
[49] J.E. Gulley, V. Jaccarino, Phys. Rev. B: Condens. Matter 6 (1972) 58.
[50] D. Skrzypek, E. Malicka, A. Cichón., J. Phys. Chem. Solids 72 (2011) 730.